Exchange-anisotropy-induced intrinsic distortion, structural transition, and rotational transition in skyrmion crystals

Xuejin Wan, Yangfan Hu,* and Biao Wang*
Sino-French Institute of Nuclear Engineering and Technology, Sun Yat-sen University, 510275 GZ, China

(Received 14 September 2018; published 21 November 2018)

Magnetic skyrmions are topologically protected noncollinear spin textures. Their condensed state, called skyrmion crystal phase (SkX), is usually presumed to be hexagonally symmetric as observed in most helimagnets. However, careful study of the experimental results indicates the existence of intrinsic anisotropy of SkX, reflected by breaking of SkX hexagonal symmetry, direction-dependent properties of SkX, and even the appearance of novel emergent crystalline states. Here, we systematically study the effects of exchange anisotropy on Bloch-type SkX in cubic helimagnets and provide a possible explanation to the phenomena mentioned above. By energy minimization, we find that exchange anisotropy causes intrinsic distortion of SkX. As the magnitude of exchange anisotropy changes, a triangular-square transition occurs, with two possible transition paths for different choices of anisotropy parameters. We also reproduce the 30° rotational transition of SkX.

DOI: 10.1103/PhysRevB.98.174427

Introduction. Magnetic skyrmions, nontrivial topologically protected vortexlike spin textures, are now of great interest because of their peculiar physical properties and potential applications as information carriers [1–7]. They have been theoretically predicted many years ago [8,9] and were first observed by the small-angle neutron scattering (SANS) experiment as a condensed phase called skyrmion crystal phase (SkX) in 2009 [10]. SkX always possesses intrinsic anisotropy in experiments. This is mainly manifested in the following aspects: (i) Intrinsic distortion of the skyrmion lattice: In the SANS experiment in MnSi [10], where no in-plane anisotropic field was applied, the intensities of two Bragg spots were obviously weaker than those of the other four; in other SANS experiments [11–13], this difference of Bragg intensities also appeared. (ii) Structural transition of SkX: Recently, a triangular-square structural transition of SkX was observed in chiral magnets $Co_8Zn_8Mn_4$ [14] and MnSi [15], where such a transition is closely related to variation of anisotropy energies [16–19]. (iii) Reorientation and 30° rotation of skyrmion lattice. In most of the SANS experiments, skyrmion lattices were reoriented with respect to the crystallographic lattice [10,20–23]. In Cu_2OSeO_3, another peculiar direction-dependent property of SkX, 30° rotation of the skyrmion lattice, was observed [11,24].

Deformation of the skyrmion lattice consists of two parts: shape deformation (called external deformation) and inequality of Bragg intensities (called internal deformation). By far, much attention has been paid to the former in experiment [25,26], theory [27], and simulation [28]. On the contrary, there is no work devoted to the explanation of the latter. Concerning the cause of structural transition of SkX, Monte Carlo simulations [17–19,29] and the analytical method [16] have found various anisotropy energies which can stabilize square SkX. However, Monte Carlo simulations cannot give an analytical description for the skyrmion magnetization structure, and the analytical method used in [16] cannot describe deformed SkX. It is widely accepted that the reorientation of skyrmion lattice results from the sixth-order anisotropic magnetocrystalline coupling. However, whether this mechanism can be used to explain the 30° rotation of SkX remains an open question. Moreover, concerning all these different aspects of the anisotropic properties of SkX, a generally effective theoretical model is not seen.

In this work, we establish a model of exchange anisotropy for cubic helimagnets with the symmetry of a T point group and try to explain the phenomena mentioned above. First, we construct the mean-field-based free-energy-density model with exchange anisotropy (including two terms characterized by the rescaled coefficients $\widetilde{A}_{e1}$ and $\widetilde{A}_{e2}$) considered and establish a unified Fourier representation for SkX. Here, unified means that (i) it unfreezes deformation-related degrees of freedom and thus it is suitable not only for triangular and square SkXs but also for deformed SkX; (ii) it is suitable for Bloch SkX [10,30], Néel SkX [31,32], anti-SkX [33], and their dipole versions (dipole Bloch SkX, see Refs. [34,35]) induced by different types of Dzyaloshinskii–Moriya interactions (DMIs). Then, by energy minimization, we demonstrate that negative exchange anisotropy can stabilize SkX and result in intrinsic distortion of the skyrmion lattice. We investigate the triangular-square structure transition procedure and find two transition paths induced by $\widetilde{A}_{e1}$ and $\widetilde{A}_{e2}$. By plotting the $\widetilde{A}_{e1}$-$\widetilde{A}_{e2}$ phase diagram at appropriate conditions of temperature and magnetic field, we find a 30° rotation of skyrmion lattice.

Model. The free energy density used here is the rescaled one [36–39],

$$\widetilde{\omega} = \sum_{i=1}^{3}\left(\frac{\partial \mathbf{m}}{\partial r_i}\right)^2 - 2\mathbf{b}\cdot\mathbf{m} + 2\mathbf{m}\cdot(\nabla\times\mathbf{m}) + t\mathbf{m}^2 + \mathbf{m}^4 + \widetilde{\omega}_{\mathrm{e}}, \tag{1}$$

*Corresponding author: huyf3@mail.sysu.edu.cn; wangbiao@mail.sysu.edu.cn

where $\mathbf{m}$, $\mathbf{b} = [0,\ 0,\ b]^{\mathrm{T}}$ and t represent, respectively, the rescaled magnetization, magnetic field, and temperature; $\widetilde{\omega}_{\mathrm{e}}$ is the rescaled exchange anisotropy, consisting of two terms $\widetilde{\omega}_{\mathrm{e}1} = \widetilde{A}_{\mathrm{e}1}[(\frac{\partial m_1}{\partial r_1})^2 + (\frac{\partial m_2}{\partial r_2})^2 + (\frac{\partial m_3}{\partial r_3})^2]$ and $\widetilde{\omega}_{\mathrm{e}2} = \widetilde{A}_{\mathrm{e}2}[(\frac{\partial m_1}{\partial r_2})^2 + (\frac{\partial m_2}{\partial r_3})^2 + (\frac{\partial m_3}{\partial r_1})^2]$. One should notice that other types of anisotropy, such as uniaxial anisotropy which can stabilize SkX [40], are not considered here. The magnetization texture of deformed SkX is described by n-order Fourier expansion [41]:

$$\mathbf{m}_{\mathrm{sk}} = \mathbf{m}_0 + \sum_{i=1}^{n}\sum_{j=1}^{n_i} \mathbf{m}_{\mathbf{q}_{ij}} e^{i\mathbf{q}_{ij}^{\mathrm{d}}\cdot\mathbf{r}}. \tag{2}$$

Here, $\mathbf{m}_0 = [0,\ 0,\ m_0]^{\mathrm{T}}$ is the averaged magnetization along the z axis, $i\ (1,\ 2, \ldots,\ n)$ represents the order of Fourier series, and n_i stands for the number of ith-order waves. $\mathbf{q}_{ij}$ and $\mathbf{q}_{ij}^{\mathrm{d}}$ are the undeformed and deformed wave vectors connected by [42,43]

$$\mathbf{q}_{ij}^{\mathrm{d}} = \begin{bmatrix} 1+\varepsilon_{11}^{q} & \varepsilon_{12}^{q}+\omega^{q} \\ \varepsilon_{12}^{q}-\omega^{q} & 1+\varepsilon_{22}^{q} \end{bmatrix} \mathbf{q}_{ij}, \tag{3}$$

where ε_{11}^{q}, ε_{22}^{q}, ε_{12}^{q}, and ω^{q} respectively reflect the elongation of the x axis, y axis, the shear deformation of the xy plane, and the rotation of the xy plane along the z axis in reciprocal space. $\mathbf{m}_{\mathbf{q}_{ij}}$ denotes the wave polarization and can be expressed as

$$\mathbf{m}_{\mathbf{q}_{ij}} = \sum_{k=1}^{3} c_{ijk}\mathbf{P}_{ijk}, \tag{4}$$

where $c_{ijk} = c_{ijk}^{\mathrm{re}} + ic_{ijk}^{\mathrm{im}}\ (k = 1,\ 2,\ 3)$ are complex parameters, $\mathbf{P}_{ij1} = \frac{1}{\sqrt{2}s_i q}[-iq_{ijy},\ iq_{ijx},\ s_i q]^{\mathrm{T}}$, $\mathbf{P}_{ij2} = \frac{1}{s_i q}[q_{ijx},\ q_{ijy},\ 0]^{\mathrm{T}}$, $\mathbf{P}_{ij3} = \frac{1}{\sqrt{2}s_i q}[iq_{ijy},\ -iq_{ijx},\ s_i q]^{\mathrm{T}}$, with $s_i q$ the wavelength of ith-order undeformed waves. As to the mathematical description for the conical phase, three parameters are enough, $\mathbf{m}_{\mathrm{conical}} = [m_q\cos(qz),\ m_q\sin(qz),\ m_3]^{\mathrm{T}}$.

Stabilization and intrinsic distortion of SkX. By substituting the magnetization textures $\mathbf{m}_{\mathrm{sk}}$ and $\mathbf{m}_{\mathrm{conical}}$ into $\widetilde{\omega}_{\mathrm{e}1}$, we find it null for $\mathbf{m}_{\mathrm{conical}}$ while negative for $\mathbf{m}_{\mathrm{sk}}$ if $\widetilde{A}_{\mathrm{e}1} < 0$. Therefore, a negative $\widetilde{A}_{\mathrm{e}1}$ favors SkX. By plotting the b-t phase diagram, we find that SkX is stabilized within a pocketlike region for low exchange anisotropy $\widetilde{A}_{\mathrm{e}1}$ [Fig. 1(a)]. As to $\widetilde{\omega}_{\mathrm{e}2}$, a negative $\widetilde{A}_{\mathrm{e}2}$ will induce the energy density for both conical phase and SkX. Actually, only for $\widetilde{A}_{\mathrm{e}2}$ with high strength can SkX be stabilized as a ground state. Figure 1(b) shows the b-t phase diagram for $\widetilde{A}_{\mathrm{e}2} = -0.8$, and we see that SkX exists in a region far away from the phase transition line between the ferromagnetic phase and single-Q phase. Another point we should notice is that the Curie temperature changes due to the presence of $\widetilde{A}_{\mathrm{e}2}$. To explain this, we solve analytically the phase transition line between the ferromagnetic phase and single-Q phase and get $b = \frac{1}{2+\widetilde{A}_{\mathrm{e}2}}\sqrt{2(t_{\mathrm{C}} - t)}$ with the Curie temperature $t_{\mathrm{C}} = \frac{2}{2+\widetilde{A}_{\mathrm{e}2}}$.

$\widetilde{\omega}_{\mathrm{e}1}$ and $\widetilde{\omega}_{\mathrm{e}2}$ are not invariant under the sixfold rotational symmetry operations. Therefore, with $\widetilde{\omega}_{\mathrm{e}1}$ and $\widetilde{\omega}_{\mathrm{e}2}$ considered, the hexagonal symmetry of SkX is broken. Figures 1(c) and 1(e) [1(d) and 1(f)] show the magnetization structure of SkX

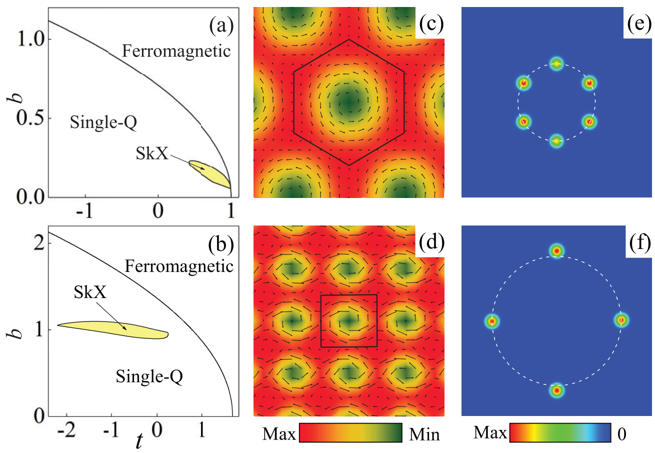

FIG. 1. b-t phase diagram for (a) $\widetilde{A}_{\mathrm{e}1} = -0.05$, $\widetilde{A}_{\mathrm{e}2} = 0$ and (b) $\widetilde{A}_{\mathrm{e}1} = 0$, $\widetilde{A}_{\mathrm{e}2} = -0.8$. The single-Q phase consists of the in-plane type (helical) and the out-of-plane type (conical). Magnetization structure of SkX at (c) $b = 0.1$, $t = 0.8$, $\widetilde{A}_{\mathrm{e}1} = -0.05$, and $\widetilde{A}_{\mathrm{e}2} = 0$, (d) $b = 1$, $t = -1$, $\widetilde{A}_{\mathrm{e}1} = 0$, and $\widetilde{A}_{\mathrm{e}2} = -0.8$. The region encircled by black lines is a skyrmion Wigner-Seitz cell. The arrows represent the distribution of the in-plane components of magnetization, and the colored density plot illustrates the distribution of the out-of-plane components of magnetization m_z. (e, f) First-order Bragg spots corresponding to (c) and (d).

and the first-order Bragg spots at $b = 0.1$, $t = 0.8$, $\widetilde{A}_{\mathrm{e}1} = -0.05$, and $\widetilde{A}_{\mathrm{e}2} = 0$ [$b = 1$, $t = -1$, $\widetilde{A}_{\mathrm{e}1} = 0$, and $\widetilde{A}_{\mathrm{e}2} = -0.8$]. In Figs. 1(c) and 1(e), the skyrmion lattice is almost hexagonal, while the intensities of six spots exhibit inequality. In Figs. 1(d) and 1(f), the intensities of four spots is almost the same, while the wavelengths along the x and y axes are different. This means that exchange anisotropy can induce intrinsic distortion of the skyrmion lattice. Actually, in many of the SANS experiments [11,12,21], the observed spots have different intensities, which may be explained by our results.

During the calculation, the in-plane single-Q phase, whose magnetization structure can also be described by Eq. (2), appears as the ground state at certain $(b,\ t)$. In the b-t phase diagrams, we do not make a distinction between the out-of-plane single-Q phase and the in-plane single-Q phase and simply call them a single-Q phase. Considering both the calculation accuracy and efficiency, we have used the third-order Fourier representation of SkX for the calculation [41,44].

Triangular-square structural transition of SkX. We first investigate the evolution of SkX magnetization structure as a function of $\widetilde{A}_{\mathrm{e}1}$. To eliminate the influence of the other exchange anisotropy term $\widetilde{A}_{\mathrm{e}2}$, we set it to 0. The temperature and magnetic field are carefully chosen so that during the whole phase transition procedure, SkX has the lowest energy density compared with the other phases. Here, we set $b = 0.35$ and $t = 0.5$. For weak exchange anisotropy $\widetilde{A}_{\mathrm{e}1} = -0.25$ [Fig. 2(a)], skyrmion lattices are arranged with a triangle pitch, a quasi-hexagonal shape. As the strength of exchange anisotropy $\widetilde{A}_{\mathrm{e}1}$ increases from -0.25 to -0.4 [Fig. 2(b)], a notable deformation of skyrmion lattices occurs, which is reflected by the following two aspects: (i) the distance between the top and bottom skyrmion lattices decreases, resulting in

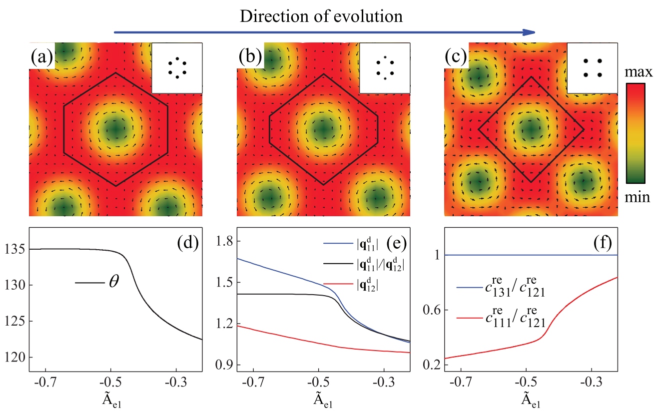

FIG. 2. Triangular-square structural transition of SkX with increasing strength of exchange $\widetilde{A}_{e1}$ at $b = 0.35$, $t = 0.5$, and $\widetilde{A}_{e2} = 0$. The upper row shows the evolution of magnetization structure as a function of $\widetilde{A}_{e1}$. From left to right, (a) $\widetilde{A}_{e1} = -0.25$, (b) $\widetilde{A}_{e1} = -0.4$, (c) $\widetilde{A}_{e1} = -0.7$. The insets in (a), (b), and (c) are the first-order Bragg spots. The lower row shows skyrmion-deformation-related parameters as functions of $\widetilde{A}_{e1}$. From left to right, (d) the angle θ between $\mathbf{q}^d_{11}$ and $\mathbf{q}^d_{12}$, (e) the wavelengths $|\mathbf{q}^d_{11}|$, $|\mathbf{q}^d_{12}|$ and their ratio $|\mathbf{q}^d_{11}|/|\mathbf{q}^d_{12}|$, and (f) the relative wave amplitudes $c^{re}_{131}/c^{re}_{121}$ and $c^{re}_{111}/c^{re}_{121}$.

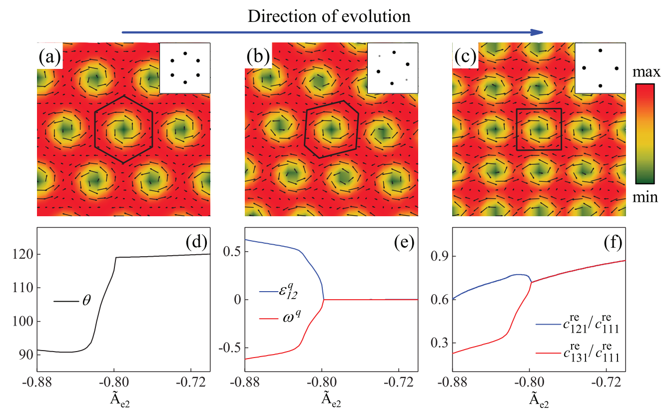

FIG. 3. Triangular-square structural transition of SkX with increasing strength of exchange $\widetilde{A}_{e2}$ at $b = 1.1$, $t = -0.8$, and $\widetilde{A}_{e1} = -0.3$. The upper row shows the evolution of magnetization structure as a function of $\widetilde{A}_{e2}$. From left to right, (a) $\widetilde{A}_{e2} = -0.76$, (b) $\widetilde{A}_{e2} = -0.81$, and (c) $\widetilde{A}_{e2} = -0.86$. The lower row shows skyrmion-deformation-related parameters as a function of $\widetilde{A}_{e2}$. From left to right, (d) the angle θ between $\mathbf{q}^d_{11}$ and $\mathbf{q}^d_{12}$, (e) the shear deformation ε^q_{12} and the rotation ω^q, and (f) the relative wave amplitudes $c^{re}_{121}/c^{re}_{111}$ and $c^{re}_{131}/c^{re}_{111}$.

the external deformation, and (ii) the intensities of top and bottom Bragg spots are obviously weaker than those of the other four [see inset of Fig. 2(b)], resulting in the internal deformation. When the strength of $\widetilde{A}_{e1}$ is increased to -0.7 [Fig. 2(c)], the distance between the top and bottom skyrmion lattices decreases further and the square pitch arrangement is formed. In this case, the top and bottom Bragg spots can be regarded as second-order ones and their intensities are much weaker than those of first-order ones. The triangular-square transition occurs as if the SkX is "compressed" along the vertical axis.

Figures 2(d)–2(f) show the evolutions of several suitable order parameters which describe this transition as functions of $\widetilde{A}_{e1}$ at $b = 0.35$, $t = 0.5$, and $\widetilde{A}_{e2} = 0$. The external-deformation-related parameters are the angle θ between $\mathbf{q}^d_{11}$ and $\mathbf{q}^d_{12}$ [Fig. 2(d)], the lengths of $\mathbf{q}^d_{11}$ and $\mathbf{q}^d_{12}$, and their ratio $|\mathbf{q}^d_{11}|/|\mathbf{q}^d_{12}|$ [Fig. 2(e)]. The internal-deformation-related parameters are $c^{re}_{131}/c^{re}_{121}$ and $c^{re}_{111}/c^{re}_{121}$ [Fig. 2(f)]. θ varies from about 120° to about 135° with increasing strength of $\widetilde{A}_{e1}$. Once $\widetilde{A}_{e1}$ exceeds a certain value (here, about -0.47), θ remains at about 135° and $|\mathbf{q}^d_{11}|/|\mathbf{q}^d_{12}|$ reaches its saturated value $\sqrt{2}$. We conclude that the square shape of the skyrmion lattice can be kept in a certain range of $\widetilde{A}_{e1}$. For $-0.47 < \widetilde{A}_{e1} < -0.22$, $\mathbf{q}^d_{11}$ increases with increasing strength of $\widetilde{A}_{e1}$, while $\mathbf{q}^d_{12}$ keeps its value near 1; for $-0.75 < \widetilde{A}_{e1} < -0.47$, both $\mathbf{q}^d_{11}$ and $\mathbf{q}^d_{12}$ change linearly with $\widetilde{A}_{e1}$. This implies that the external deformation of skyrmion lattices during the triangular-square transition is characterized by the compression along the y axis, and once the transition is finished, it is characterized by the lattice constant decreasing. The first-order Fourier expansion coefficient c^{re}_{111} degenerates into a second-order one during the triangular-square transition, since $c^{re}_{111}/c^{re}_{121}$ decreases continuously from 0.84 ($\widetilde{A}_{e1} = -0.22$) to 0.38 ($\widetilde{A}_{e1} = -0.47$), then to 0.25 ($\widetilde{A}_{e1} = -0.75$). ω_{e1} is invariant under the mirror symmetry operation $(x, y) \rightarrow (-x, y)$, and $\mathbf{q}^d_{11}$ and $\mathbf{q}^d_{12}$ are symmetric with respect to the y axis; therefore, $c^{re}_{131}/c^{re}_{121}$ is always 1. Due to the invariance of ω_{e1} under fourfold rotation about the z axis, a magnetization distribution with fourfold rotational symmetry is favored when ω_{e1} is large. That may explain the formation of square SkX at high $\widetilde{A}_{e1}$.

Then we discuss the effect of $\widetilde{A}_{e2}$ and find that it leads to another triangular-square structural transition path, as illustrated in Fig. 3. Here, we set $\widetilde{A}_{e1} = -0.3$ to suppress the conical phase so that SkX is the ground state during the transition procedure. In the interval $-0.8 < \widetilde{A}_{e2} < -0.7$, θ is about 120°, ε^q_{12} and ω^q are 0, while $c^{re}_{121}/c^{re}_{111}$ and $c^{re}_{131}/c^{re}_{111}$ vary with $\widetilde{A}_{e2}$, suggesting that the skyrmion lattice goes through only the internal deformation. For $-0.89 < \widetilde{A}_{e2} < -0.8$, θ decreases from 120° to 90° with increasing strength of $\widetilde{A}_{e2}$; on the other hand, ε^q_{12} and ω^q are no longer 0. Therefore, the triangular-square transition procedure is achieved by share deformation and rotation. We also note that c^{re}_{121} is not equal to c^{re}_{131} for nonzero ε^q_{12} and ω^q. The reason is that, in this case, $\mathbf{q}^d_{11}$ and $\mathbf{q}^d_{12}$ are not symmetric with respect to the y axis. $\widetilde{\omega}_{e2}$

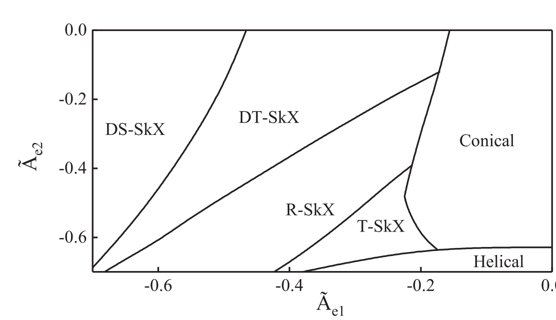

FIG. 4. $\widetilde{A}_{e1}$-$\widetilde{A}_{e2}$ phase diagram at $b = 0.5$ and $t = -0.5$.

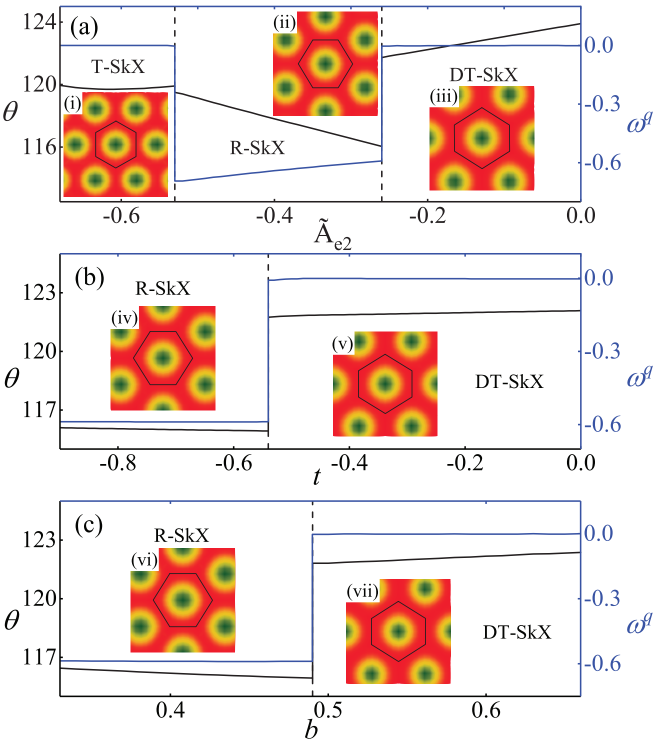

FIG. 5. (a) θ and ω^q as functions of $\widetilde{A}_{e2}$ at $b = 0.5$, $t = -0.5$, and $\widetilde{A}_{e1} = -0.3$ The insets show the m_z distribution at (i) $\widetilde{A}_{e2} = -0.6$, (ii) $\widetilde{A}_{e2} = -0.4$, and (iii) $\widetilde{A}_{e2} = -0.2$. They correspond to, from right to left, DT-SkX, R-SkX, and T-SkX, respectively. (b) θ and ω^q as functions of t at $b = 0.5$, $\widetilde{A}_{e1} = -0.3$, and $\widetilde{A}_{e2} = -0.25$. The insets (iv) and (v) show the m_z distribution for $t = -0.6$ and $t = -0.3$, respectively. (c) θ and ω^q as functions of b at $t = -0.5$, $\widetilde{A}_{e1} = -0.3$, and $\widetilde{A}_{e2} = -0.25$. The insets (vi) and (vii) show the m_z distribution for $b = 0.4$ and $b = 0.6$, respectively.

includes two nonzero terms for SkX, $(\frac{\partial m_1}{\partial r_2})^2$ and $(\frac{\partial m_3}{\partial r_1})^2$. For negative $\widetilde{A}_{e2}$, the first term tends to align the skyrmion cores along the y axis so that m_1 varies more sharply along the y axis, while the second term tends to align the skyrmion cores along x axis. That is the reason why the square SkX has $\mathbf{q}_{11}^{\mathrm{d}}$ along the y axis and $\mathbf{q}_{12}^{\mathrm{d}}$ along the x axis.

$\widetilde{A}_{e1}$-$\widetilde{A}_{e2}$ phase diagram. By plotting the $\widetilde{A}_{e1}$-$\widetilde{A}_{e2}$ phase diagram at $b = 0.5$, $t = -0.5$ (Fig. 4), we find six different phases: the conical phase, helical phase, deformed triangular SkX (DT-SkX), rotated SkX (R-SkX), triangular SkX (T-SkX), and deformed square SkX (DS-SkX). At low $\widetilde{A}_{e1}$, the ground state is a conical (helical) phase when $\widetilde{A}_{e2}$ is low (high). At moderate $\widetilde{A}_{e1}$, the conical and helical phases are suppressed and SkX appears. In this case, the shape of the skyrmion lattice changes continuously with $\widetilde{A}_{e1}$ and $\widetilde{A}_{e2}$ when $\widetilde{A}_{e2}$ is low, while it keeps the hexagon form (θ is about 120°, $|\mathbf{q}_{11}^{\mathrm{d}}|/|\mathbf{q}_{12}^{\mathrm{d}}|$ is about 1) when $\widetilde{A}_{e2}$ is high. We distinguish these two kinds of SkXs and call them deformed triangular SkX and triangular SkX, respectively. The DT-SkX and T-SkX are separated by another phase, which is formed by rotating $\mathbf{q}_{11}^{\mathrm{d}}$ and $\mathbf{q}_{12}^{\mathrm{d}}$ about 30° along the z axis [see inset (ii) of Fig. 5(a)]. We call this intermediate phase rotated SkX. At high $\widetilde{A}_{e1}$, the square SkX is formed, and the skyrmion lattice deforms continuously within certain ranges of $\widetilde{A}_{e1}$ and $\widetilde{A}_{e2}$. We refer to this phase as deformed square SkX.

We fix $\widetilde{A}_{e1} = -0.3$ and plot Fig. 5(a), which shows θ and ω^q as functions of $\widetilde{A}_{e2}$. It is shown that the phase transitions between DT-SkX and R-SkX, and between R-SkX and T-SkX, are characterized by the 30° rotation of the skyrmion lattice along the z axis. The 30° rotation of the skyrmion lattice has been observed in Cu_2OSeO_3 [24], but it occurred due to temperature or magnetic field change. In Figs. 5(b) and 5(c), we plot θ and ω^q as functions of t and b. We find that by changing the temperature and magnetic field, the 30° rotation of the skyrmion lattice occurs.

Conclusion. In conclusion, we show that SkX possesses intrinsic distortion due to the exchange anisotropy terms $\widetilde{A}_{e1}$ and $\widetilde{A}_{e2}$. In addition, we reveal two different paths for the triangular-square structural transition, which are characterized by (i) elongation and (ii) shear deformation and rotation of wave vectors. Moreover, we reproduce another phase transition of SkX, which is achieved through rotation of SkX along the z axis about 30°.

Acknowledgments. The work was supported by the NSFC (National Natural Science Foundation of China) through funds No. 11772360, No. 11832019, No. 11472313, and No. 11572355 and the Pearl River Nova Program of Guangzhou (Grant No. 201806010134).

[1] T. Schulz, R. Ritz, A. Bauer, M. Halder, M. Wagner, C. Franz, C. Pfleiderer, K. Everschor, M. Garst, and A. Rosch, Nat. Phys. **8**, 301 (2012).
[2] K. Litzius, I. Lemesh, B. Krüger, P. Bassirian, L. Caretta, K. Richter, F. Büttner, K. Sato, O. A. Tretiakov, J. Förster *et al.*, Nat. Phys. **13**, 170 (2017).
[3] W. Jiang, X. Zhang, G. Yu, W. Zhang, X. Wang, M. B. Jungfleisch, J. E. Pearson, X. Cheng, O. Heinonen, K. L. Wang *et al.*, Nat. Phys. **13**, 162 (2017).
[4] F. Jonietz, S. Mühlbauer, C. Pfleiderer, A. Neubauer, W. Münzer, A. Bauer, T. Adams, R. Georgii, P. Böni, R. A. Duine *et al.*, Science **330**, 1648 (2010).
[5] X. Zhang, M. Ezawa, and Y. Zhou, Sci. Rep. **5**, 9400 (2015).
[6] S. Luo, M. Song, X. Li, Y. Zhang, J. Hong, X. Yang, X. Zou, N. Xu, and L. You, Nano Lett. **18**, 1180 (2018).
[7] R. Tomasello, E. Martinez, R. Zivieri, L. Torres, M. Carpentieri, and G. Finocchio, Sci. Rep. **4**, 6784 (2014).
[8] A. N. Bogdanov and D. Yablonskii, Zh. Eksp. Teor. Fiz. **95**, 178 (1989) [Sov. Phys. JETP **68**, 101 (1989)].
[9] A. Bogdanov and A. Hubert, J. Magn. Magn. Mater. **138**, 255 (1994).
[10] S. Mühlbauer, B. Binz, F. Jonietz, C. Pfleiderer, A. Rosch, A. Neubauer, R. Georgii, and P. Böni, Science **323**, 915 (2009).
[11] K. Makino, J. D. Reim, D. Higashi, D. Okuyama, T. J. Sato, Y. Nambu, E. P. Gilbert, N. Booth, S. Seki, and Y. Tokura, Phys. Rev. B **95**, 134412 (2017).

[12] T. Adams, S. Mühlbauer, A. Neubauer, W. Münzer, F. Jonietz, R. Georgii, B. Pedersen, P. Böni, A. Rosch, and C. Pfleiderer, J. Phys.: Conf. Ser. **200**, 032001 (2010).
[13] J. White, K. Prša, P. Huang, A. Omrani, I. Živković, M. Bartkowiak, H. Berger, A. Magrez, J. Gavilano, G. Nagy *et al.*, Phys. Rev. Lett. **113**, 107203 (2014).
[14] K. Karube, J. White, N. Reynolds, J. Gavilano, H. Oike, A. Kikkawa, F. Kagawa, Y. Tokunaga, H. M. Rønnow, Y. Tokura *et al.*, Nat. Mater. **15**, 1237 (2016).
[15] T. Nakajima, H. Oike, A. Kikkawa, E. P. Gilbert, N. Booth, K. Kakurai, Y. Taguchi, Y. Tokura, F. Kagawa, and T.-h. Arima, Sci. Adv. **3**, e1602562 (2017).
[16] J.-H. Park and J. H. Han, Phys. Rev. B **83**, 184406 (2011).
[17] S. Oh, H. Kwon, and C. Won, J. Korean Phys. Soc. **62**, 924 (2013).
[18] S.-Z. Lin, A. Saxena, and C. D. Batista, Phys. Rev. B **91**, 224407 (2015).
[19] S. Do Yi, S. Onoda, N. Nagaosa, and J. H. Han, Phys. Rev. B **80**, 054416 (2009).
[20] W. Münzer, A. Neubauer, T. Adams, S. Mühlbauer, C. Franz, F. Jonietz, R. Georgii, P. Böni, B. Pedersen, M. Schmidt *et al.*, Phys. Rev. B **81**, 041203 (2010).
[21] T. Adams, S. Mühlbauer, C. Pfleiderer, F. Jonietz, A. Bauer, A. Neubauer, R. Georgii, P. Böni, U. Keiderling, K. Everschor *et al.*, Phys. Rev. Lett. **107**, 217206 (2011).
[22] L. Bannenberg, F. Qian, R. Dalgliesh, N. Martin, G. Chaboussant, M. Schmidt, D. L. Schlagel, T. A. Lograsso, H. Wilhelm, and C. Pappas, Phys. Rev. B **96**, 184416 (2017).
[23] Y. Luo, S.-Z. Lin, D. Fobes, Z. Liu, E. Bauer, J. Betts, A. Migliori, J. Thompson, M. Janoschek, and B. Maiorov, Phys. Rev. B **97**, 104423 (2018).
[24] S. Seki, J.-H. Kim, D. Inosov, R. Georgii, B. Keimer, S. Ishiwata, and Y. Tokura, Phys. Rev. B **85**, 220406 (2012).
[25] K. Shibata, J. Iwasaki, N. Kanazawa, S. Aizawa, T. Tanigaki, M. Shirai, T. Nakajima, M. Kubota, M. Kawasaki, H. Park *et al.*, Nat. Nanotechnol. **10**, 589 (2015).
[26] C. Wang, H. Du, X. Zhao, C. Jin, M. Tian, Y. Zhang, and R. Che, Nano Lett. **17**, 2921 (2017).
[27] A. Leonov and I. Kézsmárki, Phys. Rev. B **96**, 214413 (2017).
[28] S.-Z. Lin and A. Saxena, Phys. Rev. B **92**, 180401 (2015).
[29] A. Leonov, Twisted, localized, and modulated states described in the phenomenological theory of chiral and nanoscale ferromagnets, Ph.D. thesis, Technical University of Dresden, 2011.
[30] S. Seki, X. Yu, S. Ishiwata, and Y. Tokura, Science **336**, 198 (2012).
[31] T. Kurumaji, T. Nakajima, V. Ukleev, A. Feoktystov, T.-h. Arima, K. Kakurai, and Y. Tokura, Phys. Rev. Lett. **119**, 237201 (2017).
[32] I. Kézsmárki, S. Bordács, P. Milde, E. Neuber, L. Eng, J. White, H. M. Rønnow, C. Dewhurst, M. Mochizuki, K. Yanai *et al.*, Nat. Mater. **14**, 1116 (2015).
[33] A. K. Nayak, V. Kumar, T. Ma, P. Werner, E. Pippel, R. Sahoo, F. Damay, U. K. Rößler, C. Felser, and S. S. Parkin, Nature (London) **548**, 561 (2017).
[34] S. Montoya, S. Couture, J. Chess, J. Lee, N. Kent, M.-Y. Im, S. Kevan, P. Fischer, B. McMorran, S. Roy *et al.*, Phys. Rev. B **95**, 224405 (2017).
[35] S. Montoya, S. Couture, J. Chess, J. Lee, N. Kent, D. Henze, S. Sinha, M.-Y. Im, S. Kevan, P. Fischer *et al.*, Phys. Rev. B **95**, 024415 (2017).
[36] P. Bak and M. H. Jensen, J. Phys. C **13**, L881 (1980).
[37] U. Rößler, A. Bogdanov, and C. Pfleiderer, Nature (London) **442**, 797 (2006).
[38] A. O. Leonov and A. N. Bogdanov, New J. Phys. **20**, 043017 (2018).
[39] See Supplemental Material at http://link.aps.org/supplemental/10.1103/PhysRevB.98.174427 for details of the calculation method.
[40] A. Butenko, A. Leonov, U. Rößler, and A. Bogdanov, Phys. Rev. B **82**, 052403 (2010).
[41] Y. Hu and B. Wang, New J. Phys. **19**, 123002 (2017).
[42] M. Born and K. Huang, *Dynamical Theory of Crystal Lattices* (Clarendon Press, Oxford, 1954).
[43] Y. Hu and B. Wang, arXiv:1608.04840.
[44] Y. Hu, Commun. Phys. **1**, 82 (2018).